Trans. Phenom. Nano Micro Scales, 2(2): 86-99, Summer – Autumn 2014
DOI: 10.7508/tpnms.2014.02.001

ORIGINAL RESEARCH PAPER

The Impact of Nanoparticles on Forced Convection in a Serpentine Microchannel

P. Rahim Mashaei[1,*], S. M. Hosseinalipour[1], M. El Jawad Muslmani[1]
[1]Mechanical Engineering Department, Iran University of Science & Technology (IUST), Tehran, I.R. Iran

ARTICLE INFO.

Article history
Received 13 Septembre 2013
Accepted 1 June 2014

Keywords
Al_2O_3 Water
Nanofluid
Thermal Conductivity
Viscosity

Abstract

In this study heat transfer and fluid flow characteristics of Al_2O_3/water nanofluid in a serpentine microchannel is numerically investigated. A constant heat flux is applied on microchannel wall and a single-phase model has been adopted using temperature-dependent properties. The effects of pertinent factors such as Reynolds number (Re=10, 20, 50 and 100), particle volume fraction (Φ=0(distilled water), 2, 4 and 8%) and heat flux (q=5, 10 and 15 W/cm^2), on the velocity and temperature field, average heat transfer coefficient (h_{avg}), pressure drop (Δp), and thermal-hydraulic performance (η) are evaluated. The results show that the use of nanofluid causes increased velocity gradient near the wall which is more remarkable for φ = 8%. The results also reveal that the heat transfer rate increases as nanoparticle volume fraction and Reynold number increase and a maximum value 51% in the average heat transfer coefficient is detected among all the considered cases when compared to basefluid (i.e., water). It is found that a higher heat flux leads to heat transfer enhancement and reduction in pressure drop. Finally, thermal-hydraulic performance is calculated and it is seen that the best performance occurs for Re =10 and φ = 4%.

1. Introduction

Microchannels have attracted a lot of research efforts in two recent decades because of the need to achieve rapid heat transfer in microfluidics-based devices. These devices are used in various engineering applications such as chemical,biochemical, electronic, aerospace and automotive industries. Microchannels feature remarkably high heat transfer rate and low thermal resistance [1]. However, a restrictive factor for the heat transfer in a microchannel is associated to the working fluid transport properties. In order to solve this problem, the fluid properties must be improved. Recently, with the development of manufacturing technology, the production of nano-particles has become possible. Addition of these nano-particles into the conventional cooling fluids such as water, oil and ethylene glycol has created a special class of fluid, called 'nanofluid' [2]. Many researchers have reported the increase of the thermal conductivity in nanofluids and different reasons have been proposed to explain it. Wang et al. [3] proposed that the thermal conductivity of nanofluids depends on microscopic motion and particle structure. Xuan and

[*]Corresponding author
Email address: Payam.Mashaei@Gmail.Com

Nomenclature

∇	Nabla operator (1/m)	U_{in}	Inlet velocity (m/s)
B_c	Boltzman constant	w	Channel width
C_p	Specific heat of the fluid (J/kg K)		**Greek Symbols**
d	Size of particle or molecule(m)	α	Thermal diffusivity
H	Channel height (m)	η	Thermal-hydraulic performance factor
h	heat transfer coefficient through the heat sources (W/m^2 K)	μ	Dynamic viscosity (Pa.s)
		ρ	Density (kg/m^3)
k	Thermal conductivity (W/m K)	ϕ	Particle volume fraction (%)
k_B	Boltzmann constant (J/K)		**Subscripts**
l	Mean free path (m)	w	wall conditions
Nu	local Nusselt Number ($Nu = \frac{qH}{k(T_w - T_m)}$)	ave	average
p	Pressure (Pa)	bf	base fluid
q	Heat flux of heat sources (W/m2)	nf	nanofluid
Re	Reynolds number ($\mathrm{Re} = \frac{\rho_{nf} u_{in} D_h}{\mu_{nf}}$)	p	particles
S	Curvilinear coordinate (m)	r	ratio
T	Temperature (K)	0	inlet conditions
V	Velocity vector (m/s)		

Li [4] also discussed two reasons for the enhanced thermal conductivity of nanofluids: the increased thermal dispersion due to the disorganized movement of suspended nanoparicles and the increased thermal conductivity of nanofluids. Lee et al. [5] investigated that Al_2O_3 water/ethylene glycol with particle diameters 24.4 and 38.4 nm as well as CuO-water/ethylene glycol with particle diameters 18.6 and 23.6 nm and showed that thermal conductivity increases to 20% as particle volume fraction increases from 0 to 4%. Chopkar el al. [6] measured thermal conductivity of Ag_2Al-water nanofluids and Al_2Cu water nanofluids and found that it increases by about 130% with a volume fraction less than 2%. Several investigators [7-9] found that the thermal conductivity of nanofluids depends on both volume fraction and temperature. They showed that the thermal conductivity of nanofluids significantly increases as temperature rises. Based on this feature of nanofluids, Mashaei et al. [10,11] suggested that they may be used as a smart material in cooling of hot spots. These authors carried out a numerical analysis of the flow and heat transfer characteristics of nanofluid in a parallel plates channel with discrete heat sources. The heat sources were placed on the bottom wall at a constant heat flux and remaining channel surfaces were considered adiabatic. They reported that the use of the nanofluid can produce an asymmetric velocity along the height of the channel and the wall temperature decreases, especially near the hot spot, where heat sources are located.

With respect to the problem under study that is heat transfer and pressure drop characteristics of nanofluid flow through microchannel, there are numerous works [12-25], which consider such a problem.

Yang and Lai [12] performed mathematical modeling to simulate forced convection flow of Al_2O_3/water nanofluids in a microchannel using the lattice Boltzmann method (LBM) for low Reynolds numbers (Re<16). They reported that the average Nusselt number increases with the increase of Reynolds number and particle volume concentration, and the fluid temperature distribution is more uniform with the use of a nanofluid than that of pure water. Mohammed et al. [13] numerically investigated the performance of a counter-flow rectangular shaped microchannel heat exchanger (MCHE) using nano-fluids as the working fluids. They stated that the increase in nanoparticle volume fraction yields better

performance at the expense of increased pressure drop. Chen and Ding [14] presented the problem of forced convection heat transfer in a microchannel heat sink with pure water and water-based nanofluids containing Al_2O_3 nanoparticles by modeling the microchannel as a fluid-saturated porous medium. They reported that the temperature distribution of the channel wall is practically insensitive to the inertial effect, while the fluid temperature distribution and the total thermal resistance alter remarkably due to the inclusion of flow inertial force. Tokit et al. [15] numerically studied an interrupted microchannel heat sink (IMCHS) using nanofluids as working fluids. They investigated the effects of the transport properties, nanofluid type, nanoparticle volume fraction and particle diameter on the IMCHS performance and found that the highest thermal augmentation is predicted for Al_2O_3, followed by CuO, and finally for SiO_2 in the IMCHS. These authors also reported that the Nu number increased with the increase of nanoparticle volume fraction and with the decrease of nanoparticle diameter. Koo and Kleinstreur [16] simulated laminar nanofluid flow in microchannels and showed that the addition of nanoparticles, e.g., CuO-particles of mean diameter dp = 20 nm at low volume fractions, to high-Prandtl number liquids remarkably increases the heat transfer performance of micro heat-sinks. Raisi et al. [17] numerically studied the thermal performance of a microchannel considering the effect of both slip and no-slip conditions on the flow field and heat transfer. They concluded that the heat transfer rate is remarkably affected by the nanoparticle volume fraction and slip coefficient at high Reynolds number. Kalteh et al. [18] considered an Eulerian two-fluid model to simulate the nanofluid flow inside the microchannel and observed that the relative velocity and temperature between the phases is very small and negligible and the nanoparticle concentration distribution is uniform. They also stated that the two-phase modeling results show higher heat transfer enhancement in comparison to the homogeneous single-phase model. Chein and Chung [19] experimentally investigated that the better heat transfer rate for CuO-water nanofluid in a microchannel compared to the basefluid may be obtained only at low coolant flow rates.

Fani et al. [20] investigated nanoparticles size effects on thermal performance and pressure drop of a nanofluid in a trapezoidal microchannel-heat-sink (MCHS). They reported that by increasing volume concentration, nanoparticles size effect becomes more prominent and it is observed that increment rate of pressure drop is intensified for above 150 nm particles diameter. Unlike the pressure drop, heat transfer decreases with an increase in nanoparticles diameter. Also, these authors observed that with an increase in nanoparticles diameter, average Nusselt number of base fluid decreases more than that of the nanoparticles and this signifies that base fluid has more efficacy on thermal performance of copper-oxide nanofluid. Hasan [21] analyzed flow and heat transfer characteristics in a micro pin fin heat sink with two types of nanofluids (Diamond-water and Al_2O_3-water) in addition to the pure water. He showed that the use of nanofluid instead of pure fluid as a coolant leads to enhanced heat transfer performance by increasing the amount of heat dissipated but it also leads to increased pressure drop for all fins shapes and nanofluids studied. Halelfadle et al. [22] focused on analytical optimization of a rectangular microchannel heat sink using aqueous carbon nanotubes based nanofluid as coolant. They showed that use of the nanofluid as a working fluid reduce the total thermal resistance and can enhance significantly the thermal performances of the working fluid at high temperatures. Singh et al. [23] investigated heat transfer behavior of nanofluids in microchannel with hydraulic diameters 218 and 303 μm. They found that better heat transfer characteristics can be obtained by higher concentration of nanofluids and by low viscous base fluids. Jung et al. [24] and Ho et al. [25] experimentally showed that Al_2O_3-water nanofluid outperformed water as the transport media due to higher heat transfer rate.

To the best knowledge of authors, there is no work to investigate the effect of nanofluid on the serpentine microchannel performance. Thus the present study deals with three dimensional simulations of the laminar nanofluid flow and heat transfer characteristics through a serpentine microchannel considering temperature-dependent properties. Results of interest such as profiles of nanofluid properties, temperature distribution, velocity profiles, heat transfer coefficient, pressure drop, and thermal-hydroulic performance as a function of particle volume fraction are discussed in this paper.

2. Geometry Configuration

In the present study the velocity and temperature fields are determined in a serpentine microchannel, as

shown in Figure 1. This serpentine microchannel is made of a succession of 90^0 sharp bends. The cross-section is a rectangle with an aspect ratio 2 (100μm × 200μm). Thus the microchannel hydraulic diameter is 133.33μm. The unfolded length of the channel is 5.4mm. As the maximum heat transfer rate occurs where the flow changes its direction [26], the profiles are investigated at the last turn, as marked in Figure 1.

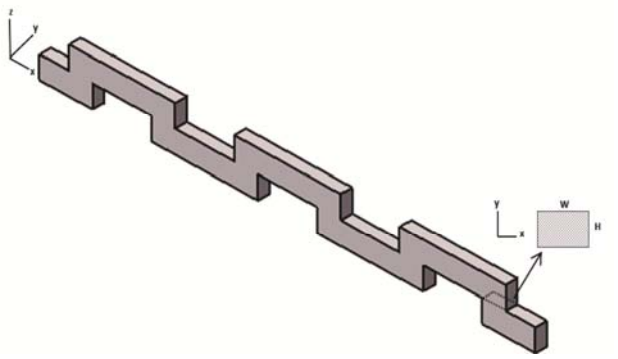

Fig. 1. Considered serpentine microchannel.

3. Governing Equations and Boundary Conditions

particles, it is expected that the nanoparticles and basefluid are in thermal equilibrium and they flow at same velocity.

In the present study, the nanofluid is considered incompressible withtemperature-dependent properties. The compression work and viscous dissipation terms were considered negligible in the energy equation. Under such assumptions, the general governing equations are written as follow.

Conservation of mass:

$$\nabla.\boldsymbol{V} = 0 \tag{1}$$

Conservation of momentum:

$$\nabla.(\rho_{nf}\boldsymbol{VV}) = -\nabla P + \nabla.(\mu_{nf}\nabla\boldsymbol{V}) \tag{2}$$

Conservation of energy:

$$\nabla.(\rho_{nf}\boldsymbol{V}(C_p)_{nf}T) = \nabla.(k_{nf}\nabla T) \tag{3}$$

Equations 1 to 3 are solved by using appropriate boundary conditions. The flow boundary conditions are a fully developed velocity profile at the channel inlet, no-slip at the channel walls and zero relative pressure at the channel outlet. As the mean free path for liquid molecules is 0.1-1 nm, the channel hydraulic diameter should be smaller than 1μm to be in the slip region [27].Thus the no-slip condition on the microchannel wall is a reasonable assumption to make for reasonable in this study. The mean velocity at inlet depends on the Reynolds number and the nanoparticle volume fractions given in Table 1 For thermal boundary conditions, a uniform temperature (295 K) is imposed at the channel entrance and a fixed heat flux is applied on microchannel wall.

Table 1
Mean velocities at inlet

Re	Φ=0 (Water)	Φ=2%	Φ=4%	Φ=8%
10	0.075	0.083	0.088	0.17
20	0.15	0.166	0.177	0.34
50	0.375	0.415	0.444	0.851
100	0.75	0.83	0.888	1.703

4. Nanofluid Thermophysical Properties

The thermo-physical properties of the nanofluid are mainly functions of nanoparticle volume fraction and temperature [28]. In the absence of experimental data, nanofluid density and specific heat are defined only as a function of volume fraction:

Density:

$$\rho_{nf} = (1-\phi)\rho_{bf} + \phi\rho_p \tag{4}$$

Specific heat:

$$(C_P)_{nf} = (1-\phi)(C_P)_{bf} + \phi(C_p)_p \tag{5}$$

In the above equations, subscripts 'bf', 'p' and 'nf' refer to basefluid, nanoparticle and the nanofluid, respectively. Also Φ is the volume fraction of the nanoparticles. The effective viscosity of the Al_2O_3/water nanofluid with the nanoparticle diameter (d_p) equal to 47 nm is calculated from the relation presented in [29] based on data obtained in [30]:

$$\mu_{nf} = 0.001(-0.155 - \frac{19.582}{T} + 0.794\varphi + \frac{2094.47}{T^2} \tag{6}$$

$$-0.192\varphi^2 - 8.11\frac{\varphi}{T} - \frac{27563.863}{T^3} + 0.0127\varphi^3 + 1.6044\frac{\varphi^2}{T} + 2.1754\frac{\varphi}{T^2})$$

In this simulation, the thermal conductivity considers Brownian motion and mean diameter of the nanoparticles, defined as [31]:

$$\frac{k_{nf}}{k_{bf}} = 1 + 64.7\phi^{0.7466}\left(\frac{d_{bf}}{d_p}\right)^{0.3690}\left(\frac{k_p}{k_{bf}}\right)^{0.7476}\left(\frac{2.4\times10^{-5}\times10^{\frac{247}{T-140}}}{\rho_{bf}\,\alpha_{bf}}\right)^{0.9955}\left(\frac{\rho_{bf}\,B_c T}{3\pi(2.4\times10^{-5}\times10^{\frac{247}{T-140}})^2 l^2_{bf}}\right)^{1.2321} \quad (7)$$

Where l_{bf} is the mean free path of the basefluid and the value of 0.17 nm is considered for water. B_c and α_{bf} are the Boltzmann constant and the basefluid thermal diffusivity. d_{bf} and d_p are the basefluid molecule size and nanoparticle diameter, respectively.

5. Numerical Method

The governing differential equations are solved using the finite-volume method. These equations were discretized by the power-law scheme. The SIMPLE procedure is chosen to determine the pressure from the continuity equation. The solution convergence is met when the normalized residuals reached 10^{-6} for all the equations. In order to assess the grid independence of numerical solution, a grid independence test is carried out where five types of mesh are checked. The effect of grid size on the averaged heat transfer coefficient for Re=100 and φ = 8% is illustrated in Figure 2. As it can be seen 930741 (21×41×1081) nodes provides satisfactory solution for the shown example.

6. Results and Discussion

The thermal performance of the channel is characterized in terms of an averaged heat transfer coefficient along the microchannel unfold length, h_{ave}, defined as:

$$h_{ave} = \frac{\int h_s dS}{0.0054} \quad (8)$$

Which S is the curvilinear coordinate and 0.0054 m is the unfolded length of the microchannel in meter.

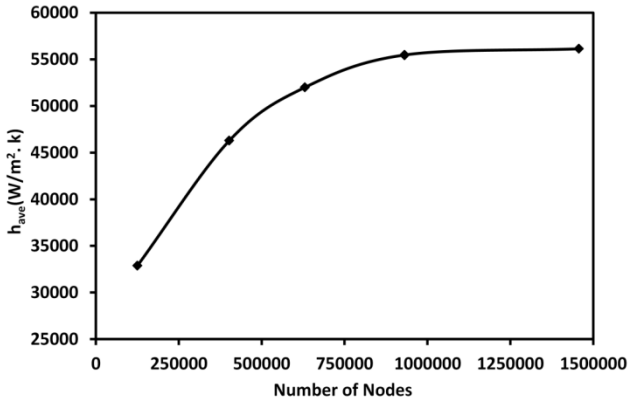

Fig. 2. Grid independence study for Re=100 and φ = 8%.

Which S is the curvilinear coordinate and 0.0054m is the unfolded length of the microchannel in meter. The local heat transfer coefficient, h_s, is given by :

$$h_s = \frac{q}{(T_b - T_w)} \quad (9)$$

Where q and T_w are the applied heat flux and the microchannel wall temperature, respectively. Also, Tb is the bulk temperature of fluid over the cross-section area of the microchannel.

The thermal-hydraulic performance factor is defined as:

$$\eta = \frac{h_r}{(\Delta P)_r^{1/3}} \quad (10)$$

Where h_r and Δp_r are respectively the average heat transfer coefficient and the pressure drop ratio, referred to values obtained for the basefluid.

6.1. Code validation

In order to prove the validity and also accuracy of the model and numerical method, two comparisons with the available data are carried out. The first comparison is related to a mini serpentine channel that all its walls are heated with a constant heat flux and the water is utilized as fluid working. In this case, the Nusselt number is compared which is given by the following definitions:

$$Nu = \frac{qD_h}{k(T_w - T_m)} \tag{11}$$

where D_h is hydraulic diameter of channel. This comparison is illustrated in Figure 3. It is seen that the results of the present study are in a good agreement with the numerical results of Lasbet et al.[26].The second comparison is concerned with the local Nusselt number through a microchannel with Re=6.9 and φ=5%. Figure 4 shows remarkable agreement between the present results on the local Nusselt number and those provided by Islami et al.[32].

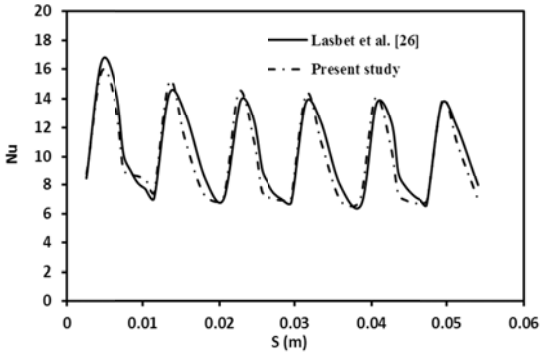

Fig. 3. Comparison of present numerical results with those obtained by Lasbet et al. (2007).

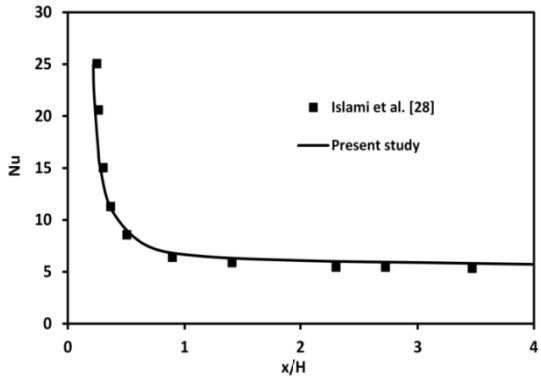

Fig. 4. Comparison of the local Nusselt number between present simulation and numerical results (Islami et al.2013) for water-Al_2O_3 nanofluid with Re=6.9 and φ =5% in microchannel.

6.2. Variation of Nanofluid Properties

As the nanofluid properties were considered temperature-dependent, their variation may play a significant role in flow and heat transfer characteristics of nanofluid forced convection through the microchannel. Figure 5a and b show thermal conductivity of nanofluid on the wall along the microchannel for Re=10 and 100, respectively. According to these figures, it can be seen that the local nanofluid thermal conductivity increases with a wavy behavior along the microchannel for all cases and the maximum local thermal conductivity may be detected on the microchannel wall at the outlet. This is due this fact that the nanofluid temperature increases as fluid flows toward the microchannel outlet. With comparison of Figure 5a and b, one can easily see that thermal conductivity illustrates higher values for Re=10. In fact, the lower flow rate increases residence time of nanofluid in microchannel more remarkably, therefore the temperature and thermal conductivity rises with higher rate. The slope of the local thermal conductivity for Re=100 (see Figure 5b) is approximately similar for all particle volume fractions, while the local thermal conductity for Re=10 (see Figure 5a) increases with various rate at different particle volume fractions. The reason of this phenomenon is explained as follows. As the nanoparticle volume fraction increases, the inlet velocity increases at a fixed Reynolds number, as well as the thermal conductivity. Therefore the increasing rate of nanofluid temperature decreases and the local thermal conductivity may increase with lower rate, as shown for φ=8% in Figure 5a.

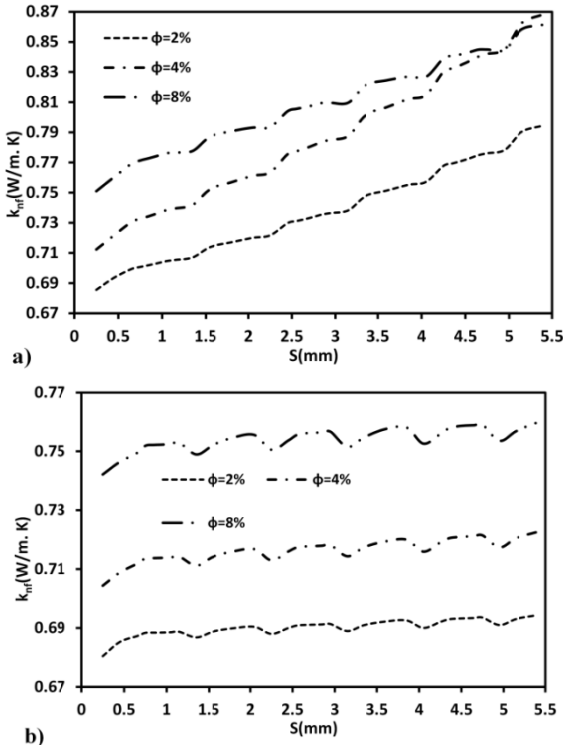

Fig. 5. Effect of particle loading parameter φ on nanofluid conductivity profile along the channel for: (a) Re = 10, (b) Re = 100.

This issue becomes more important when the flow rate is lower and the temperature variation along the microchannel is more remarkable.

The thermal conductivity profiles along the horizontal direction of the cross section located at S=4.95 mm are depicted in Figure 6a and b. They are provided for various particle volume fractions and two Reynolds numbers, equal to 10 and 100. It is shown that the thermal conductivity variation is more marked at Re=10 and the maximum values occur on the wall because of higher temperature. It also can be seen that the values of thermal conductivity are close to each other for φ=4 and 8% at Re=10. This is due to two opposite roles played by inlet velocity and thermal conductivity, both growing with particle volume fraction. Increased inlet velocity decreases temperature and thermal conductivity, especially for lower Reynolds number, while, on the other hand, thermal conductivity is increasing because of increased nanoparticle loading

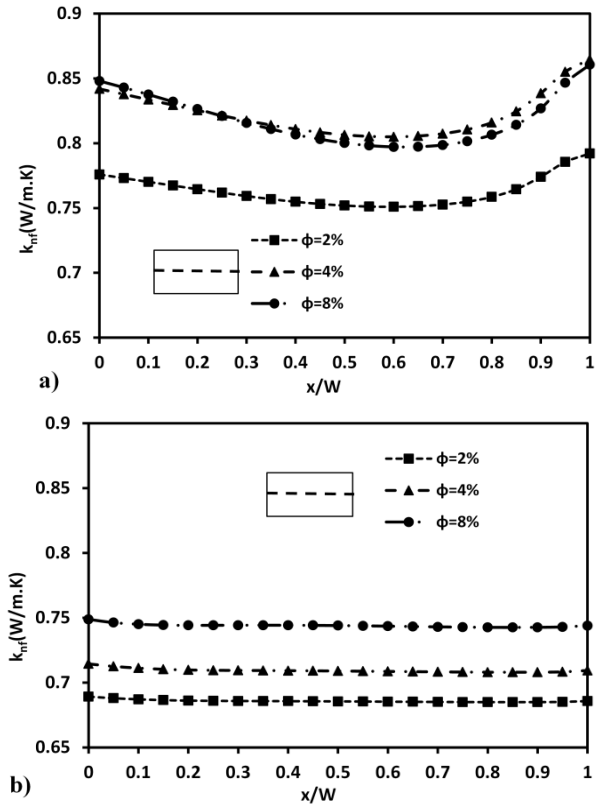

Fig. 6. Effect of particle loading parameter φ on nanofluid conductivity profile along horizontal direction of cross section at S=4.95 mm for: (a) Re = 10, (b) Re = 100.

The thermal conductivity profiles along the vertical direction of the cross section located at S=4.95 mm are illustrated in Figure 7a and b. According to these figures, for Re=100, the thermal conductivity increases as the particle volume fractions increases, while, for Re=10, the highest values of thermal conductivity are depicted at φ=4%. This is due this fact that the higher inlet velocity demonstrably decreases temperature at Re=10 and φ=8.

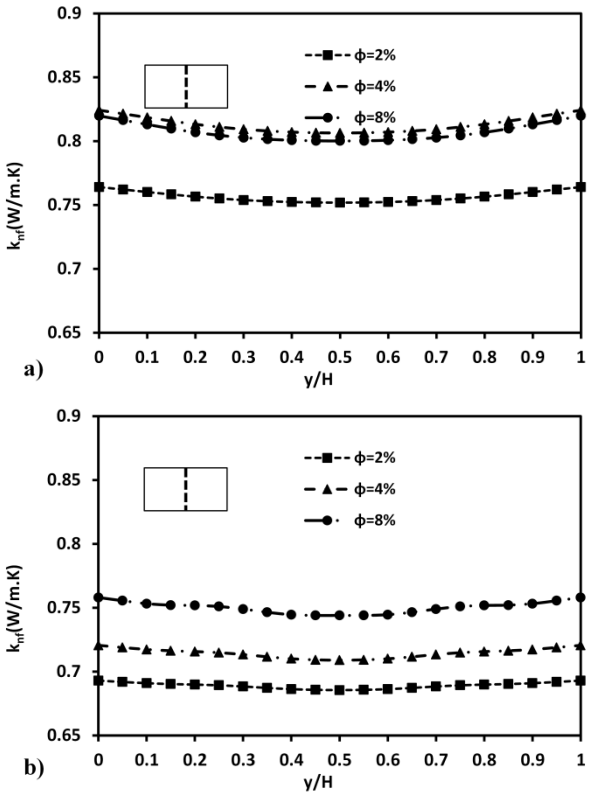

Fig. 7. Effect of particle loading parameter φ on nanofluid conductivity profile along vertical direction of cross section at S=4.95 mm for: (a) Re = 10, (b) Re = 100.

Results in term of the local dynamic viscosity are illustrated in Figure 8a and b for Re=10 and Re=100, respectively. They are given for different particle volume fractions, equal to 2, 4 and 8%. It is obviously shown than the profiles have a wavy and decreasing behavior for all considered cases. As shown in these figures, the slope of the profiles related to Re=100 are shallower due to slower rate of temperature rise.The dynamic viscosity profiles along the horizontal direction of the cross section located at S=4.95 mm are depicted in Figure 9a and b for Re=10 and 100, respectively. It can be seen that the dynamic viscosity variation is not remarkable except for Re=10 and φ=8%. This is due this fact that Al_2O_3-water nanofluid with φ=8% is strongly affected by the temperature, as

discussed in [29]. Figure 10a and b show the dynamic viscosity profiles along the vertical direction of the cross section located at S=4.95 mm. These profiles are provided for various particle volume fractions and two Reynolds number, equal to 10 and 100.

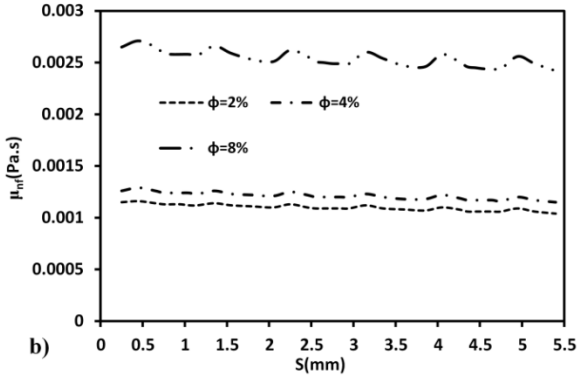

Fig. 8. Effect of particle loading parameter φ on nanofluid dynamic viscosity profile along the channel for: (a) Re = 10, (b) Re = 100.

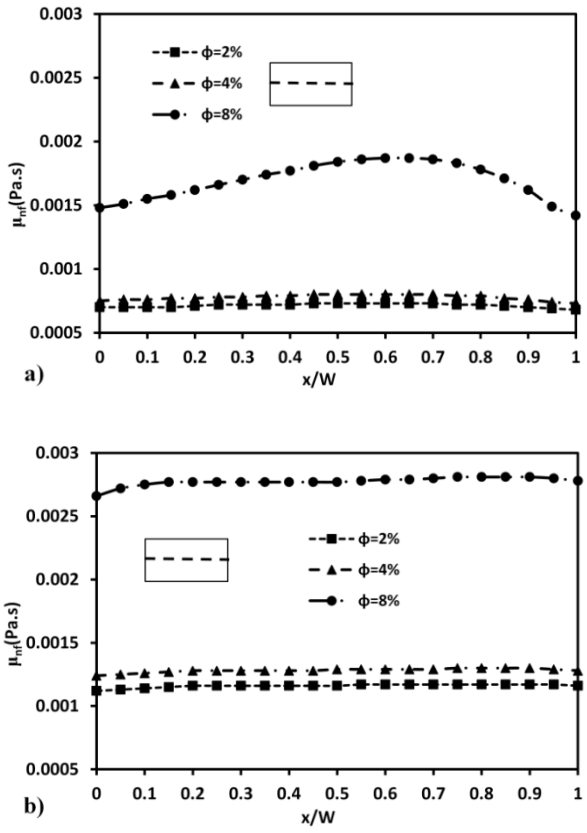

Fig. 9. Effect of particle loading parameter φ on nanofluid dynamic viscosity profile along horizontal direction of cross section at S=4.95 mm for: (a) Re = 10, (b) Re = 100.

It is noted that the dynamic viscosity profiles have lower values on the wall and the pick of viscosity profiles occurs in the middle.

By comparison of Figure 10a and b, it is observed that the dynamic viscosity gradient is more for Re=100 because of higher temperature gradient in the vertical direction for higher Reynolds number.

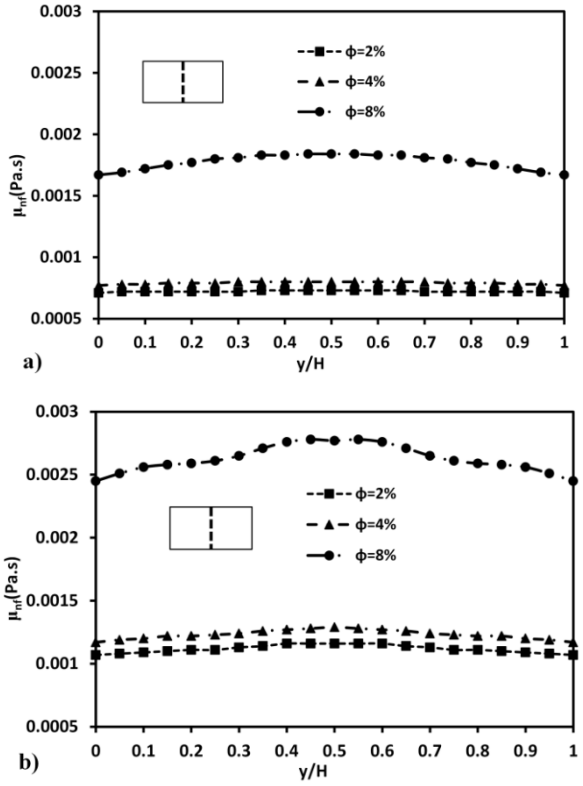

Fig. 10. Effect of particle loading parameter φ on nanofluid dynamic viscosity profile along vertical direction of cross section at S=4.95 mm for: (a) Re = 10, (b) Re = 100.

6.3. Velocity Field

The values of velocity along horizontal direction of the cross section at S=4.95 mm for Re=10 and Re=100 are depicted in Figure 11a and b, respectively, for considered volume fractions. It can be seen that with the increase of nanoparticle loading, as it is expected, the peak of velocity profile will increase. This produces larger velocity gradient near the wall which can lead an increased wall shear stress and higher pressure drops, as discussed in our previous study [10, 11]. Results in term of velocity profile along vertical direction of the cross section at S=4.95mm are shown in Figure 12a and b for Re=10 and Re=100, respectively.

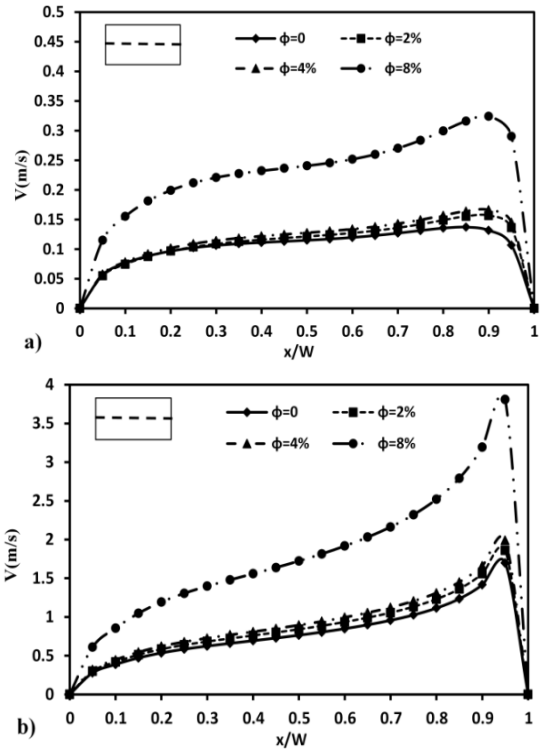

Fig. 11. Effect of particle loading parameter φ on velocity profile along horizontal direction of cross section at S=4.95 mm for: (a) Re = 10, (b) Re = 100.

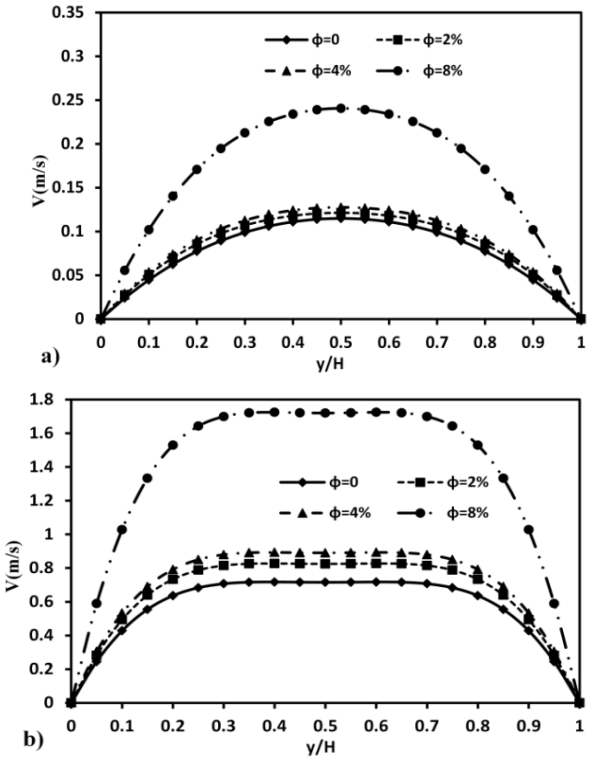

Fig. 12. Effect of particle loading parameter φ on velocity profile along horizontal direction of cross section at S=4.95 mm for: (a) Re = 10, (b) Re = 100.

One can see that the velocity profiles are flatter for Re=100 in comparison with Re=10 for all particle volume fractions. The reason can be explained as follows.

The velocity profile illustrated in Figure12 is related to the cross-section of the last turn of microchannel, where the secondary flow has a vital role in velocity and temperature fields. As the Reynolds number is increased the intensity of secondary flow and the transverse momentum transfer increase. This leads to a flatter profile for the main component of velocity.

6.4. Temperature Field and Heat Transfer

Figure 13a and b illustrate the temperature profiles along the vertical direction of the cross section located at S=4.95 mm. These profiles are given for various particle volume fractions and two Reynolds numbers, equal to 10 and 100. It is obvious that the temperature is lower for higher volume fraction because of increased thermal conductivity and inlet velocity. According to these figures, the uniformity of the temperature increases as particle volume fraction and Reynolds number increase.

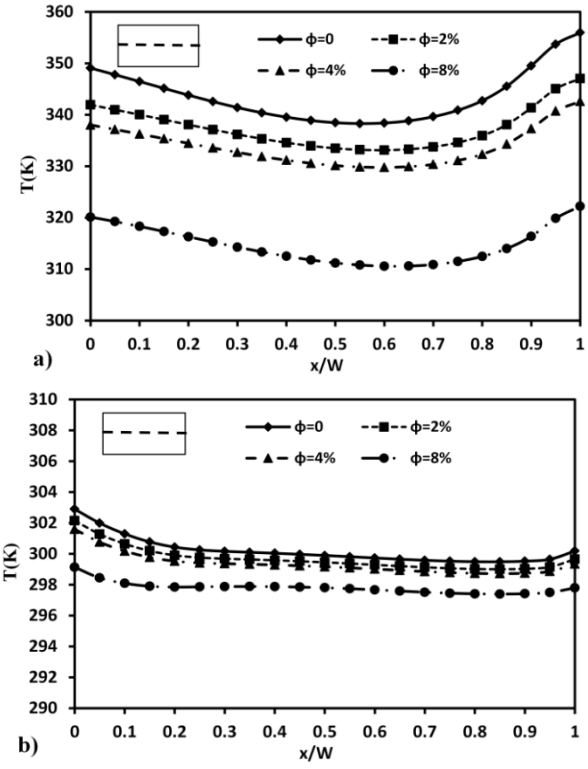

Fig. 13. Effect of particle loading parameter φ on the temperature profile along horizontal direction of cross section at S=4.95 mm for: (a) Re = 10, (b) Re = 100.

Results in term of temperature profile along vertical direction of the cross section at S=4.95mm are shown in Figure 14a and b for Re=10 and Re=100, respectively. According to these figures, we note that the temperature decreases, as particle volume fraction and Reynolds number increase. Also, one can see that the minimum value of temperature occurs at the middle of profile where is farther from microchannel walls; in fact, the lowest value of about 298K is found at y/H=0.5, Re=100 and φ=8%.

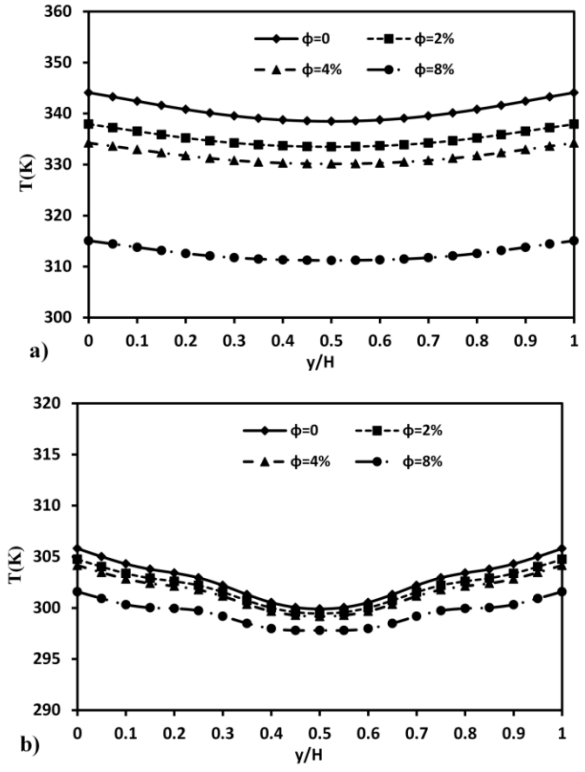

Fig. 14. Effect of particle loading parameter φ on the temperature profile along vertical direction of cross section at S=4.95 mm for: (a) Re = 10, (b) Re = 100.

Results show that the presence of nanoparticles plays a vital role in heat transfer enhancement. The average heat transfer coefficient profiles as a function of Reynolds number are illustrated in Figure 15a for φ=0, 2, 4 and 8%. In general, the average heat transfer coefficient increases as Reynolds number and particle volume fraction are increased. Thus, passing from φ = 0% to φ =8%, the maximum value of about 55476W/m^2 k for h_{ave} is detected at Re=100 and φ=8%. As we are also interested in quantifying the heat transfer augmentation advantages of nanofluids, the average heat transfer coefficient ratio, h_r, referred to the values obtained for basefluid, is shown in Fig. 15b as a function of Reynolds number for φ = 2, 4 and 8%. It can be seen that the h_r is greater than one for all considered cases and increases as particle volume fractions increases. The variation of h_r versus Reynolds number strongly depends on particle volume fraction; it will increase for φ=8% as Reynolds number increases, while decreases for φ=2 and 4%. This is due to more increased inlet velocity at φ=8%, as can be seen in Table 1. Therefore, among all considered cases, the maximum value of the average heat transfer coefficient ratio (h_r) is found at Re=100 and φ=8%.

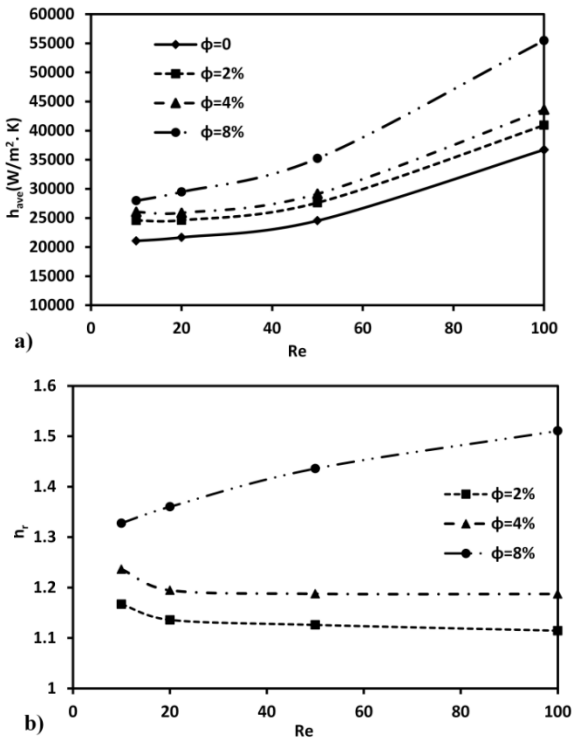

Fig. 15. Effect of parameters φ and Re on: (a) average heat transfer coefficient and (b) average heat transfer coefficient ratio.

6.5. Pressure Drop

It is expected that the use of nanoparticles in basefluid may have an adverse impact on the pressure drop because of increased viscosity. The pressure drop profiles as a function of Reynolds number are illustrated in Figure 16a for φ=0, 2, 4 and 8%. As it can be noted, the pressure drop increases as Reynolds number and particle volume fraction increase, and the highest value is found at Re=100 and φ = 8%. Figure 16b shows the pressure drop ratio, $(\Delta P)_r$, referred to the base fluid, versus Reynolds number. There is a remarkable difference between values related to

φ = 8% with those obtained for φ = 2 and 4%. As shown in this figure, the pressure drop ratio increases rapidly as Reynolds number increases for lower Reynolds numbers, while it is approximately independent of Reynolds number at higher Reynolds numbers. This is explained as follows. As the considered model for dynamic viscosity depends on temperature, the range of temperature variation along the channel affects the pressure drop. Therefore, the variation of pressure drop ratio is more pronounced at lower flow rate which causes a wider range of temperature along the microchannel.

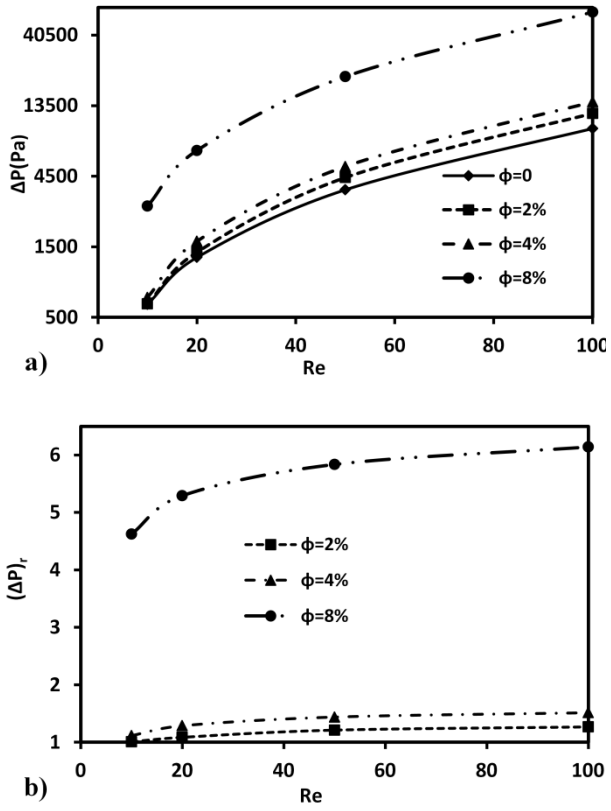

Fig. 16. Effect of parameters φ and Re on: (a) pressure drop and (b) pressure drop ratio.

6.6. Effect of Heat Flux on Heat Transfer and Pressure Drop

As microchannels may be used under a wide range of heat flux conditions and we use temperature-dependent properties, it is interesting to determine the effect of heat flux (q) on heat transfer coefficient and pressure drop. The effects of q on the average heat transfer and pressure drop are shown in Figure 17a and b, respectively. The results are provided as a function of heat flux and given for different particle volume fractions, equal to 0, 2, 4 and 8%. As illustrated in Figure 17a, one can see that the average heat transfer coefficient associated with the nanofluid increases as q is increased because of the increased nanofluid conductivity, while the average heat transfer coefficient of basefluid remains constant. On the other hand, as shown in Figure 12b, the pressure drop decreases as (q) increases, except for φ=0, because of decreased nanofluid viscosity. Therefore the use of nanofluids leads to better performance in the higher applied heat flux.

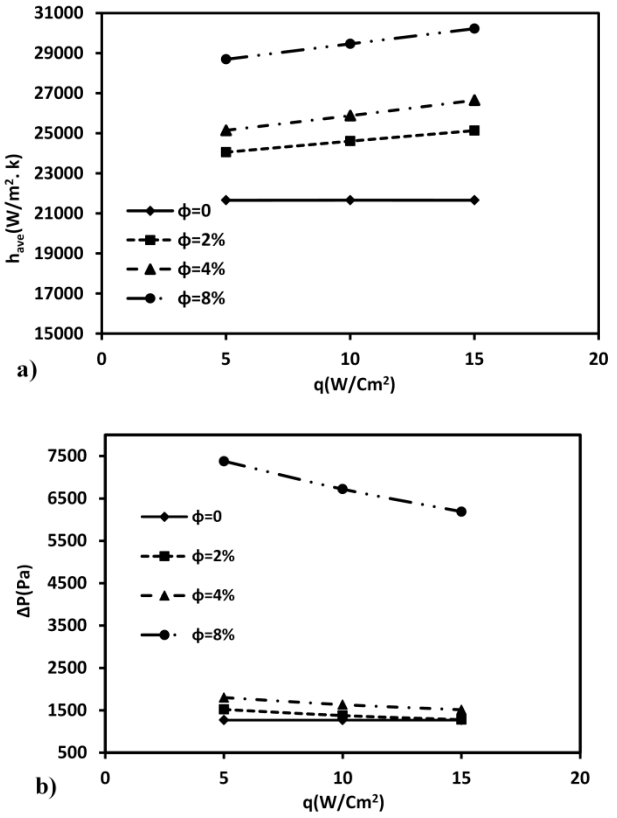

Fig. 17. Effect of parameters φ and q on (a) averaged heat transfer coefficient and (b) pressure drop.

6.7. Thermal-Hydraulic Performance

As discussed in the previous sections, the use of nanofluids increases both the heat transfer rate and pressure drop. In order to investigate the order of magnitude of the augmentation of heat transfer and the pressure drop for various Reynolds number and volume fraction, the thermal hydraulic performance factor as a function of Reynolds number is depicted in Figure 18a. It is observed that the thermal hydraulic performance has different behaviors for various particle volume fractions. For φ =2 and 4%, thermal

hydraulic performance decreases as Reynolds number increases. This is due this fact that the effect of nanofluid properties on heat transfer and fluid flow is more remarkable at lower flow rate because of considering them as a function of temperature. For φ=8%, thermal hydraulic performance decreases as Reynolds number increases from 10 to 20 and after it, the profile will increase. This behavior is due to two opposite roles played by viscosity, which is more effective at φ=8%. On the one hand, the increased viscosity improves heat transfer rate by raising the inlet velocity at a fixed Reynolds number, but on the other hand, the increase of viscosity has an adverse effect on pressure drop. The best value for thermal-Hydraulic Performance can be found at lowest Reynolds number (Re=10) and middle nanoparticle volume fraction (φ=4%). The effect of particle volume fraction on the thermal-hydraulic performance for various heat loads is shown in Figure 18b. It is clearly seen that the thermal-hydraulic performance increases as heat flux increases for all considered cases due to higher nanofluid thermal conductivity and lower nanofluid viscosity in higher temperature.

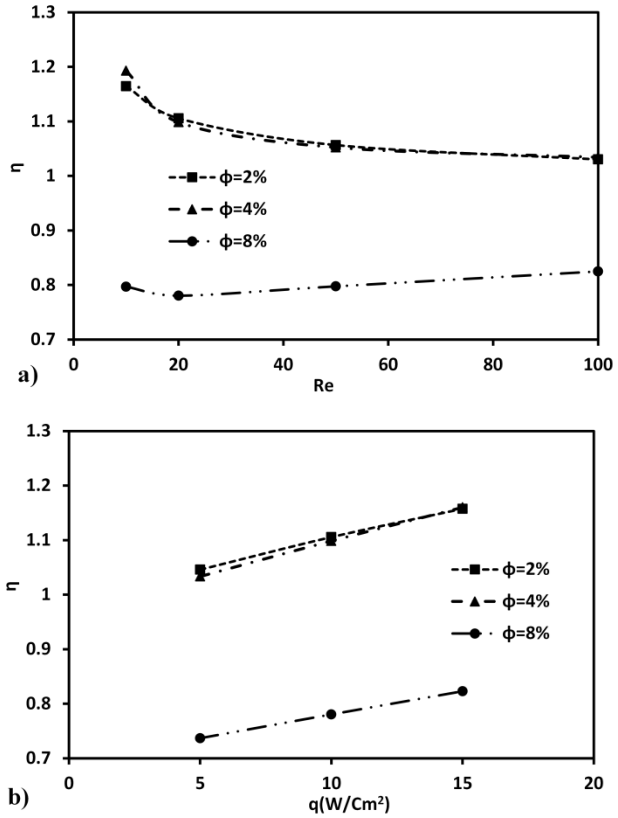

Fig. 18. (a) Effect of parameters φ and Re on η (b) Effect of parameters φ and q on η

7. Conclusion

A numerical analysis of flow and heat transfer characteristics of nanofluid in a serpentine microchannel has been presented. The basefluid is water and four volume fractions of Al_2O_3 nanoparticles (φ = 0 (distilled water) 2, 4 and 8%) are taken into account with a single-phase model. Furthermore, different Reynolds numbers in the range 10–100 and different heat fluxes in the range 5-15 W/Cm^2 are considered. Based on the results obtained, the following conclusions can be drawn:

1. The local nanofluid properties vary with a wavy behavior along the microchannel for all cases and the maximum local thermal conductivity and minimum local viscosity are detected on the microchannel wall at the outlet. Also, the variation is more pronounced for lower flow rate.
2. For all cases, the velocity values increase with increasing nanoparticle volume fraction, and consequently the velocity gradient and the shear stress on the microchannel wall increase.
3. The lowest temperature, higher heat transfer coefficient, and higher pressure drop occur at highest particle volume fraction (φ=8%) and Reynolds number (Re=100).
4. The variation of the average heat transfer coefficient ratio,(h_r), referred to the values obtained for basefluid, versus Reynolds number strongly depends on particle volume fraction; it will increase for φ=8% as Reynolds number increases, while decreases for φ=2 and 4%.
5. The pressure drop ratio rises as Reynods number increases and the growing rate of pressure drop ratio is more remarkable at lower Reynolds numbers.
6. As applied heat flux increases, the heat transfer rate improves and the pressures drop decrease.
7. The best value for thermal-Hydraulic Performance can be found at the lowest Reynolds number (Re=10) and middle nanoparticle volume fraction (φ=4%). Also, it increases linearly as heat flux increases.

Acknowledgement

We would like to express our appreciation to the Iran nanotechnology initiative council for their financial support for this project.

References

[1] C. Yang, J. Wu, H. Chein , S. Lu, Friction characteristics of water, R-134a, and air in small tubes, Microscale Thermophysical Engineering 7(2003) 335-348.

[2] S. U. S. Choi, Enhancing thermal conductivity of fluids with nanoparticles, American Society of Mechanical Engineers 66 (1995) 99–105.

[3] X. Wang, X. Xu, S.U.S. Choi, Thermal conductivity of nanoparticle-fluid mixture, Journal of Thermo- physics and Heat Transfer 13(1999) 474-480.

[4] Y. Xuan, Q. Li, Heat transfer enhancement of nano- fluids, International Journal of Heat and Fluid Flow 21 (2000) 58-64.

[5] S. Lee, S.U.S. Choi, Measuring thermal conductivity of fluids containing oxide nanoparticles, Journal of Heat Transfer 121 (1999) 280-289.

[6] I. Chopkar, S. Sudarshan, P. K. Das, I. Manna, Effect of particle size on thermal conductivity of nanofluid, Metallurgical and Material Transaction 39 (2008) 1535-1542.

[7] C. H. Li, G. P. Peterson, Experimental investigation of temperature and volume fraction variations on the effective thermal conductivity of nanoparticle suspensions (nanofluids), Journal of Applied Physics 99 (2006) 084314.

[8] S. K. Das, N. Putra, P. Thiesen, W. Roetzel, Temperature dependence of thermal conductivity enhancement for nanofluids, Journal of Heat Transfer 125 (2003) 567-574.

[9] T. P. Teng, Y. H. Hung, T. C. Teng, J. H. Chen, Performance evaluation on an air-cooled heat exchanger for alumina nanofluid under laminar flow, Nanoscale Research. Letter 6 (2011) 408.

[10] P. R. Mashaei, S. M. Hosseinalipour, M.Bahiraei, Numerical investigation of nanofluid forced convection in channels with discrete heat sources, Journal of Applied Mathematics(2012) 259-284.

[11] P. R. Mashaei, S. M. Hosseinalipour, M.Bahiraei, M.Dirani, 3-D numerical simulation of nanofluid laminar forced convection in a channel with localized heating, Australian Journal of Basic and Applied Science 6 (2012) 479-489.

[12] Y.T, Yang, F.H. Lai, Numerical study of flow and heat transfer characteristics of alumina-water nanofluids in a microchannel using the lattice Boltzmann method, International Communication of Heat and Mass Transfer 38 (2011) 607-614.

[13] H.A. Mohammed, G. Bhaskaran , N.H. Shuaib , R. Saidur, Numerical study of heat transfer enhancement of counter nanofluids flow in rectangular microchannel heat exchanger, Superlattices Microstructure 50 (2011) 215-233.

[14] C.H. Chen, C.Y. Ding, Study on the thermal behavior and cooling performance of a nanofluid-cooled microchannel heat sink, International Journal of Thermal Science 50 (2011) 378-384.

[15] E.M. Tokit, H.A. Mohammed, M.Z. Yusoff, Thermal performance of optimized interrupted microchannel heat sink (IMCHS) using nanofluids, International Communication of Heat and Mass Transfer 39 (2012) 1595-1604.

[16] J. Koo, C. Kleinstreuer, Laminar nanofluid flow in microheat-sinks, International Journal of Heat and Mass Transfer 48 (2005) 2652-2661.

[17] A. Raisi, and B.Ghasemi, M. Aminossadati, A numerical study on the forced convection of laminar nanofluid in a microchannel with both slip and no-slip conditions, Numerical Heat Transfer-Part A 59 (2011) 114-129.

[18] M. Kalteh, A. Abbassi , M. Saffar-Avval , J. Harting, Eulerian–Eulerian two-phase numerical simulation of nanofluid laminar forced convection in a microchannel, International Journal of Heat and Fluid Flow 32 (2011) 107-116.

[19] R. Chein, J.Chuang, Experimental microchannel heat sink performance studies using nanofluids, International. Journal of Thermal Science 46 (2007) 57-66.

[20] B. Fani, A. Abbassi, M. Kalteh, Effect of nano particles size on thermal performance of nanofluid in a trapezoidal microchannel-heat-sink, International Communications in Heat and Mass Transfer 45 (2013) 155–161.

[21] M.I. Hassan, Investigation of flow and heat transfer characteristics in micro pin fin heat sink with nanofluid, Applied Thermal Engineering 63 (2014) 598–607.

[22] S. Halelfadl, A. M. Adhame, N. Mohd-Ghazalib, T. Maréa, P. Estellécc, R. Ahmad, Optimization of thermal performances and pressure drop of rectangular microchannel heat

sink using aqueous carbon nanotubes based nanofluid, Applied Thermal Engineering 62 (2014) 492–499.

[23] P. K. Singh, P. V. Harikrishna, T. Sundararajan ,S. K. Das, Experimental and Numerical Investigation into the Heat Transfer Study of Nanofluids in Microchannel, Journal of Heat Transfer 133(2011) 701-709.

[24] J.Y Jung, H. S. Oh, H.Y. Kwak, Forced convective heat transfer of nanofluids in microchannels, International Journal of Heat and Mass Transfer 52 (2009) 466-472.

[25] C.J. Ho, L.C. Wei, Z.W. Li, An experimental Investigation of forced convective cooling performance of a microchannel heat sink with Al_2O_3-Water nanofluid, Applied Thermal Engineering 30 (2010) 96-103.

[26] Y. Lasbet, B. Auvity, C. Castelain, H. Peerhossaini, Thermal and hydraulic performance of chaotic microchannel: application to fuel cell cooling, Heat Transfer Engineering 28 (2007) 795-803.

[27] G.L. Morini, Viscous heating in liquid flows in micro -channel, International Journal of Heat and Mass Transfer 48 (2005) 3637-3647.

[28] A. P. Saamito, J. C. Kurnia, A. S. Mujumdar, Numerical evaluation of laminar heat transfer enhancement in nanofluid flow in coiled square tube, Nanoscale Research Letter 6 (2011) 376.

[29] E.Abu-Nada, Effect of variable and thermal conductivity of Al_2O_3-water nanofluid on heat transfer enhancement in natural convection, International Journal of Heat and Fluid Flow 30 (2009) 679-690.

[30] C.T. Nguyen, F. Desgranges, G.Roy, N. Glanis, T. Mare, S. Boucher, H. Angue Minsta, Temperature and particle size dependent viscosity data for water-based nanofluids-hystresis phenomenon, International Journal of Heat and Fluid Flow 28 (2007) 1492-1506.

[31] C.H. Chon, K.D. Kihm, Empirical correlation finding the role of temperature and particle size for nanofluid (Al2O3) thermal conductivity enhancement, Applied Physics Letter 87 (2005) 153107-1:153107-3.

[32] S. Baheri Islami, B. Dastvareh, R. Gharraei, Numerical study of hydrodynamic and heat transfer of nanofluid flow in microchannels containing micromixer, International Communication of Heat and Mass Transfer 43 (2013) 146-154.